SCIENCE CHINA Materials ARTICLES

mater.scichina.com link.springer.com

Published online 27 November 2017 | https://doi.org/10.1007/s40843-017-9141-7

Sci China Mater 2018, 61(2): 285–295

SPECIAL ISSUE: Innovative Electrode Materials for Supercapacitors

Nanotube-like hard carbon as high-performance anode material for sodium ion hybrid capacitors

Yongqiang Ding[1,2], Bingjun Yang[1], Jiangtao Chen[1], Li Zhang[3], Junshuai Li[2], Yali Li[2*] and Xingbin Yan[1*]

ABSTRACT **Sodium ion hybrid capacitors (SIHCs) are of great concern in large-scale energy storage applications due to their good energy-and-power characteristic, as well as abundant reserves and low cost of sodium. However, the sluggish faradaic kinetics of anode materials severely limit the overall electrochemical performance of SIHC devices. Herein, we report an application of nanotube-like hard carbon (NTHC) anode material prepared by high-temperature carbonization (1150°C) of polyaniline (PANI) nanotubes for high-performance SIHCs. As a result, the assembled sodium ion half-cell with NTHC shows a high reversible capacity of 419.5 mA h g^{-1} at 0.05 A g^{-1} and a good rate performance of 74.6 mA h g^{-1} at 2.5 A g^{-1} in a potential window of 0–2 V (*vs.* Na/Na^+). On this basic, a SIHC using such NTHC as anode and a high-capacity activated carbon (APDC) as cathode is fabricated, which exhibits a high energy density of 133.0 W h kg^{-1} at 2850 W kg^{-1} and still remains 100.9 W h kg^{-1} at 14,250 W kg^{-1}. Within the potential range of 1.5–3.5 V, the SIHCs display an outstanding cycling stability tested at 2 A g^{-1} with a good capacity retention of 82.5% even after 12,000 cycles.**

Keywords: sodium ion hybrid capacitor, anode, hard carbon, polyaniline, nanotube

INTRODUCTION

The ever-increasing depletion of fossil fuels has caused severe environmental pollution and other relevant issues, thus the growing demand for clean and sustainable energy is very pressing [1–4]. It is noted that, the indirect energy sources such as wind energy, solar energy and tidal energy are very promising to meet the requirements of people's daily life, but they are different greatly in geography and even change over time. So it is extremely important to develop advanced sustainable energy storage devices [5].

Electrochemical capacitors (ECs) have become the main electrochemical energy storage devices due to their high power density, long cycle life and environmental friendliness. According to different energy-storage mechanism, ECs are divided into two main categories-electrochemical double-layer capacitors (EDLCs) and the pseudo-capacitors. The former storage charge by ions reversible adsorption-desorption on the surface of the electrode materials and the latter storage energy *via* reversible Faradaic oxidation-reduction reaction over or near the surface. The development of ECs is restricted by low energy density [6–8]. On the contrary, the other type of crucial energy-storage devices such as electrochemical batteries including Li-ion [9,10], Li-O_2 [11,12], Li-S [13], Na-ion [14,15] and double-ion batteries [16,17], etc., have been extensively accepted to be durable and of high energy density to supply prolonged operation in a majority of electronic equipments. However, owing to slow insertion/extraction dynamics, these batteries show unsatisfactory power output. In recent years, a promising strategy that integrates a capacitor electrode and a battery electrode into a device has been adopted to achieve a device that has both high energy density of battery and excellent power characteristic of capacitor at the same time, such as hybrid capacitors (HCs).

As a kind of typical HCs, lithium ion hybrid capacitors (LIHCs) have been widely investigated and achieved some

[1] Laboratory of Clean Energy Chemistry and Materials, State Key Laboratory of Solid Lubrication, Lanzhou Institute of Chemical Physics, Chinese Academy of Sciences, Lanzhou 730000, China
[2] Key Laboratory of Special Function Materials & Structure Design of the Ministry of Education, Key Laboratory for Magnetism & Magnetic Materials of the Ministry of Education, and School of Physical Science & Technology, Lanzhou University, Lanzhou 730000, China
[3] Department of Physics, School of Science, Lanzhou University of Technology, Lanzhou 730050, China
* Corresponding authors (emails: xbyan@licp.cas.cn (Yan X); liyli@lzu.edu.cn (Li Y))

commercialized applications [18–22]. Unfortunately, the insufficient lithium reserves significantly restrict the further development of LIHCs. Nevertheless, the substitution of lithium with abundant sodium is a good choice to develop low-cost HCs. Such devices are viewed as so-called SIHCs and have been extensively investigated by many researchers, which are generally composed of a capacitor electrode based on activated carbon, layered oxides, phosphate and polyanion compounds, an organic polymer membrane, non-aqueous electrolyte and an anode based on carbon-based materials, metal oxides, metal sulfides, alloys [23,24]. So far, most studies were focused on seeking more suitable electrode materials for SIHCs. According to the types of anodes, various SIHCs devices have been reported, such as AC//Ti (O, N)-MP-NWs [25], Nb_2O_5@C/rGO-50//MSP [26], PSNC//PSOC [27], AC//V_2O_5/CNTs [28], $Na_3V_2(PO_4)_3$//$Na_3V_2(PO_4)_3$ [29] and N-TiO_2//AC [30]. However, the electrochemical properties of SIHCs are still limited to sluggish faradaic kinetics of anode materials, which is a major challenge for SIHCs. At present, researchers are mainly concentrating on improving the power capability of anode materials to match the fast kinetics of capacitive cathodes. The choice of the same kind of electrode materials (both as anode and as cathode) may have more excellent electrochemical performance. Carbon-based materials due to the rich resources, simple manufacturing and low cost in the SIHCs have attracted wide attention. Therefore, finding a high-performance carbon-based anode material is particularly critical for SIHCs.

PANI is a kind of conductive polymer materials. Various nanostructured PANI-based electrode materials can be obtained by different ways and have exhibited high performances for different electrochemical energy storage devices. Xu *et al.* [31] reported a hierarchical N/S-co-doped carbon anode with cellulose/PANI for sodium-ion battery, which showed a reversible capacity of 150 mA h g^{-1} in a long cycle life with 3400 cycles at 500 mA g^{-1}. Xiao *et al.* [32] reported that hollow carbon nanowires-based anode,prepared by carbonized PANI and used as an anode material for sodium ion batteries, showed a high reversible capacity of 251 mA h g^{-1} and 82.2% capacity retention after 400 cycles at 50 mA g^{-1}. Afterwards, they also prepared hard carbon nanoparticles used as anode materials with PANI for Na-ion batteries, which showed a high reversible capacity of 207 mA h g^{-1} after 500 cycles at a constant current density of 50 mA g^{-1} [33]. In our previous work, APDC with a very high specific surface area (3295 m^2 g^{-1}) could be prepared from one-dimensional PANI by a simple chemical activation [34]. Simultaneously, APDC exhibited a high capacitance and can be used as a cathode material.

In this work, we demonstrate a new SIHC utilizing a NTHC as the battery-type anode material and APDC as the capacitor-type cathode materials which are both prepared from PANI nanotubes. Specifically, NTHC can be obtained by high-temperature carbonization (1150°C) of PANI nanotubes and APDC can be obtained by KOH activation of carbonization product of PANI nanotubes. Sodium ion half-cell assembled with NTHC as anode shows a very high reversible capacity of 419.5 mA h g^{-1} at 0.05 A g^{-1} and an outstanding rate performance of 74.6 mA h g^{-1} at 2.5 A g^{-1} in voltage window of 0–2 V (*vs.* Na/Na^+). The as-built optimal SIHC shows a high energy density of 133.0 W h kg^{-1} at 2850 W kg^{-1} and exhibits high energy and power density (it still deliveries a high energy density of 100.9 W h kg^{-1} at a very high power density of 14,250 W kg^{-1}). In the voltage range of 1.5–3.5 V, this SIHC device has a very good cyclic performance at 2 A g^{-1}, in which the capacity retention rate is 82.5% after 12,000 cycles.

EXPERIMENTAL SECTION

Material preparation

All chemicals used for synthesizing PANI were commercially available and were used without further purification. Aniline (AR, 99.5%), ammonium persulfate (AR, 98.0%), citric acid (AR, 99.5%) were purchased from Sinopharm chemical reagent Co., Ltd., China.

The PANI nanotubes were synthesized by oxidative polymerization of aniline with ammonium persulfate (APS) in an aqueous solution containing citric acid according to the previous literature reports [35,36]. NTHCs were prepared by the direct carbonization of as-prepared PANI nanotubes in a tube furnace for 2 h under an argon atmosphere. The carbonization temperatures were 1050°C, 1150°C and 1250°C, respectively. The carbonized hard carbon samples were denoted as NTHC-1050, NTHC-1150 and NTHC-1250. Meanwhile, APDC was prepared by carbonization of as-prepared PANI nanotubes and then activated by KOH based our previous work [34]. Firstly, PANI nanotubes were carbonized at 800°C for 1 h under argon atmosphere at a tube furnace. Then, 0.5 g carbonized nanotubes were impregnated with 3 g KOH in a mixed solvent of 3 mL deionized water and 2 mL ethanol by evaporation at 80°C under magnetic stirring. The mixtures were dried and then heated at 800°C for 1 h under argon atmosphere. The samples were washed with

dilute hydrochloric acid and deionized water until pH=7. Finally, the samples were dried at 60°C in oven.

Material characterization

Field emission scanning electron microscope (FESEM, JSM-5601LV, Japan) was employed to investigate the microcosmic morphology of NTHC. The microstructure, chemical composition and lattice structure of as-prepared NTHC were characterized by transmission electron microscope (TEM, JEOL 2100 FEG). The structure and composition of NTHCs were investigated *via* powder X-ray diffraction (XRD, Smart APEX Ⅱ) using Cu-Kα radiation. The Raman spectra of HCNTs were obtained by Raman spectroscope (LabRAM HR Evolution) with a wavelength of 532 nm. The nitrogen adsorption-desorption isotherm measurements were carried out by an ASAP 2020 volumetric adsorption analyzer (Micromeritics, USA) at 77 K. X-ray photoelectron spectroscopy (XPS) spectra of HCNTs were measured through an X-ray photoelectron spectrometer (ESCALAB 250Xi) using monochromatic Al-Kα radiation ($h\nu$=1486.6 eV) run at 210 W.

Fabrication of sodium half cells

All the sodium half cells investigated for the material performance in this work were fabricated into coin cell. The anode was prepared by mixing 80 wt.% of NTHC, 10 wt.% of carbon black and 10 wt.% of polyvinylidene difluoride (PVDF). The mixture was coated on a Cu foil and dried at 110°C for 12 h under vacuum. After being pressed, an anode electrode was assembled into a coin cell with a counter electrode of Na using 1 mol L^{-1} $NaClO_4$ in a mixture (50:50, volume ratio) of ethylene carbonate (EC) and dimethyl carbonate (DMC) as the electrolyte in an argon-filled glove box.

Fabrication and characterization of the SIHCs

The SIHC devices were assembled with NTHC-1150 anode and APDC cathode in coin cells. For NTHC-1150 anode, the mass loading of NTHC-1150 was 1–1.5 mg. For the cathode fabrication, 90 wt.% APDC and 10 wt.% binder (polytetrafluoroethylene, PTFE) were mixed, coated on an Al foil, dried at 150°C for 12 h under vacuum and then assembled in a glove box filled with argon atmosphere. To achieve the SIHCs with the highest energy and power density, the weight ratios of anode and cathode active materials were carefully adjusted to 2:1, 1:1, 1:2 and 1:3 in the voltage range of 1.5–4.2 V, respectively.

Electrochemical measurements

All the electrochemical measurements were carried out at room temperature. Cyclic voltammetry (CV), galvanostatic charge/discharge (GCD) measurements and electrical impedance spectroscopy (EIS) were tested by the electrochemical workstations (CHI660D, Shanghai, China; and Autolab, PGSTAT 302N, Metrohm, Switzerland). The cycling charge-discharge tests of half-cells and hybrid cells were carried out using a CT2001A cell test instrument (LAND Electronic Co., Ltd., China).

The specific capacity (C, F g^{-1}) of SIHCs was calculated by the following equation:

$$C = I[(\mathrm{d}E/\mathrm{d}t)\times m] \approx I[(\Delta E/\Delta t)\times m], \quad (1)$$

where I is the constant discharge current, Δt is the time period for a full discharge, m indicates the mass of the corresponding active electrode material and ΔE represents the voltage change after a full discharge. Here the specific capacity of SIHCs was calculated based on the total mass of anode and cathode active materials.

The energy density (E, W h kg^{-1}) of SIHCs can be calculated by the specific capacity (C) and cell voltage (V_{max}-upper cutoff voltage, V_{min}-lower cutoff voltage) according to the following equation:

$$E = 0.5C\left(V_{max}^2 - V_{min}^2\right). \quad (2)$$

The power density (P, W kg^{-1}) of SIHCs can be obtained by the energy density (E) and the discharging time (t) according to the following equation:

$$P = E/t. \quad (3)$$

RESULTS AND DISCUSSION

Morphological and structural analysis

Fig. 1 is a schematic diagram of the fabrication of our dual-carbon SIHCs and working fundamental. First, the NTHC anode was prepared under argon atmosphere by high temperature carbonization process, and the APDC cathode was prepared by chemical activation with KOH (their structural properties are shown in Figs. S1 and S2). After the SIHCs was assembled, it works as follows: During the charging process, Na^+ ions are inserted the quasi-graphitic layers of NTHC and ClO_4^- ions are adsorbed on the surface of the APDC; during the discharge process, Na^+ ions are removed from the graphite layers of NTHC and ClO_4^- ions are desorbed from the surface of APDC [37].

PANI nanotubes are prepared by oxidative polymerization of aniline with APS. The as-prepared PANI exhibits a uniform tubular structure with about 80–150 nm for external diameter and around 40–50 nm

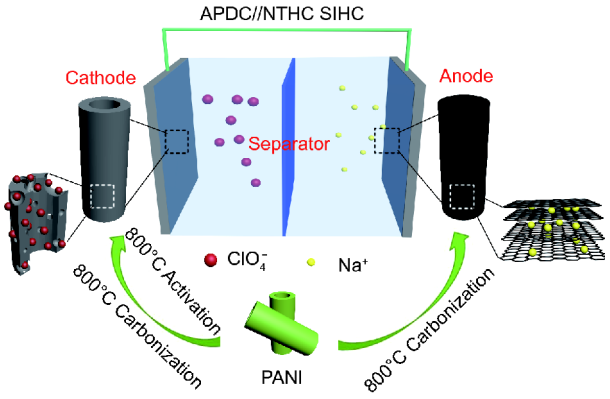

Figure 1 Schematic diagram of NTHC//APDC dual-carbon SIHC with NTHC as anode and APDC as cathode.

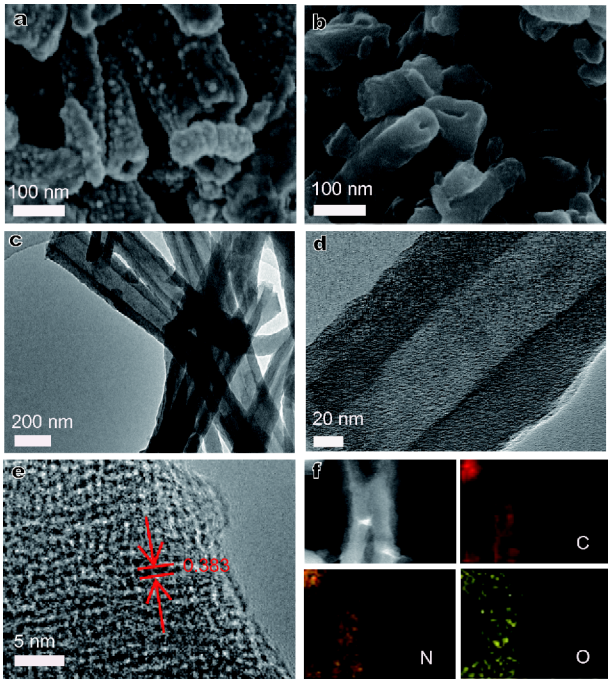

Figure 2 The SEM images of PANI precursor (a) and NTHC-1150 (b). (c, d) TEM images of NTHC-1150; (e) HRTEM of NTHC-1150; (f) element mappings of NTHC-1150.

for inner diameter (Fig. 2a). The formation of the PANI nanotubes appears, we speculate that this is related to the lower oxidative polymerization temperature. When the aniline molecules are oxidized at lower temperature, they easily form oligomers of nanocrystals by stacking mechanism. These oligomers act as templates for the adsorption of N-phenylphenazines during the induction process. Meanwhile these N-phenylphenazines are used as starting template for forming PANI nanotubes by stacking around the oligomeric nanocrystallite [38,39]. After annealing, the as-made NTHC-1150 remains hollow tubular nanostructure. Moreover, the surface becomes smoother and the diameter decreases slightly (Fig. 2b). The TEM images of the NTHC-1150 (Fig. 2c, d) show that the internal hollow tube has a diameter of ~40 nm, which is consistent with the SEM images results. The HRTEM image of NTHC-1150 in Fig. 2e shows that it consists of graphite flakes containning many disordered voids, which could provide a diffusion channel for sodium ions and electrons to improve the rate capability of NTHC-1150. The elemental mappings of carbon, nitrogen and oxygen atoms further reveal that the entire NTHC-1150 has a uniformly distributed hollow tube structure (Fig. 2f).

XRD patterns of PANI nanotubes, NTHC-1050, NTHC-1150 and NTHC-1250 are shown in Fig. 3a. The PANI nanotubes show two broad peaks centered at 2θ=19.7° and 25.4°, indicating an amorphous phase [40]. All of NTHCs have two broad peaks at ~23.5° and ~43.5°, corresponding to (002) and (101) planes, which are characteristic of amorphous carbon materials. It is worth noting that the position of the (002) peak slightly shifts to low angles as the carbonization temperature increases, which indicates the layer distance increases with increasing the pyrolysis temperature [41,42]. Moreover, according to the Bragg equation, the layer distances of NTHC-1050, -1150, -1250 in the position of the (002) plane are calculated to be 0.376, 0.383 and 0.386 nm, respectively. The value of NTHC-1150 is consistent with the HRTEM result in Fig. 2e. The increase of layer distance is probably due to the fact that more gasous atoms are inserted into/moved within the layers of graphite during the pyrolyzation at higher temperature [43]. Such larger interlayer space of NTHC is favorable for insertion and extraction of Na^+, leading to the improvement of the sodium storage capacity. Raman spectra of NTHCs as shown in Fig. 3b exhibit broad D-bands around 1350 cm^{-1} and G-bands around 1580 cm^{-1}, which could be attributed to the disorder of graphite edges and crystalline graphite [44], respectively. The ratios of the intensity of D- and G- bands could be obtained by the spectra, with I_D/I_G being employed to index the degree of graphitic ordering. The I_D/I_G of NTHC-1050, -1150, -1250 are 1.80, 1.68 and 1.44, respectively. This further confirms the amorphous nature of the carbonized NTHCs that is consistent with the XRD results. The analyses of the XRD and Raman results are shown in Table S1.

The nitrogen adsorption isotherms and pore size distribution of PANI nanotubes and NTHCs are shown in

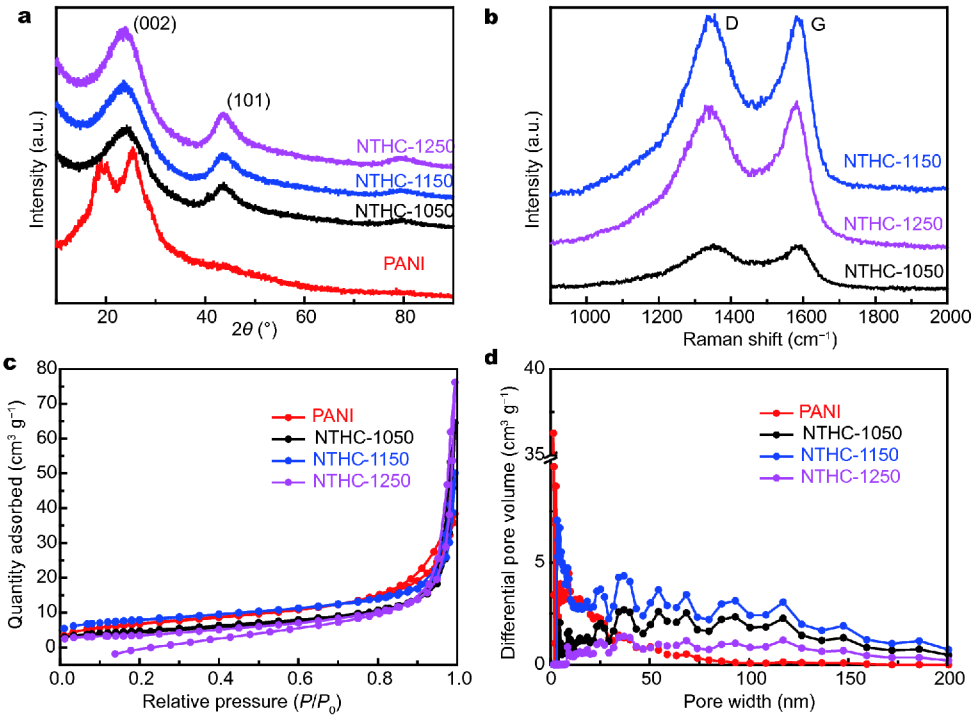

Figure 3 (a) XRD patterns of PANI and NTHCs; (b) Raman spectra of NTHCs; (c) nitrogen adsorption-desorption isotherms of PANI and NTHCs; (d) pore size distribution of PANI and NTHCs.

Fig. 3c and d. The total Brunauer-Emmett-Teller (BET) specific surface area and the total pore volume of PANI and NTHCs are listed in Table S1. The specific surface of PANI precurosr is 24.8 $m^2 g^{-1}$. As annealing temperature increases, the specific surface area of as-obtained NTHCs gradually decreases. Especially, the NTHC-1050 shows the maximum BET surface area of 26.8 $m^2 g^{-1}$, while NTHC-1150 and NTHC-1250 show smaller surface area of 17.05 and 12.56 $m^2 g^{-1}$, respectively. The analysis of pore size distribution shows that the pore distribution in all materials is relatively wide, including mesopores and macropores. The co-existence of hierarchical pores is beneficial to the transmission of electrons and the wettability of electrolyte, thus improving the rate performance and cycle stability [45,46].

XPS was employed to investigate chemical state of the nitrogen atoms in NTHCs. N 1s XPS data for the PANI precursor and NTHCs obtained at different temperatures (1050°C and 1150°C) are shown in Fig. S3. It should be noted that, when the annealing temperature reaches 1250°C, the signal of nitrogen atom for the resulting NTHC-1250 cannot be detected, indicating nitrogen atoms are almost released from the final product. The atomic percentages of N of PANI precursor, NTHC-1050 and NTHC-1150 can reach up to 8.79%, 1.23% and 1.21%, respectively. The N 1s peak of the pristine PANI (Fig. S3a) can be deconvoluted into two peaks positioned at 399.6 and 400.5 eV [47]. The N 1s peak of NTHC-1050 can be splited into two peaks and envelop the contributions from two components after fitting (Fig. S3b). The peak centered at 401 eV may be attributed to quaternary-nitrogen (N-Q) formed in the early stage of carbonization. The second peak positioned at 402.1 eV may be assigned to the nitrogen-oxide (N-O) species doped at the edges of the graphite layers. The shift towards higher binding energy for the peaks assigned to the N-Q (401.2 eV) and N-O (402.4 eV) binding implies that a slight change in the chemical environment with increased temperature. The N-Q binding can increase the conductivity of carbon materials to improve the rate performance of the battery [48]. All related results are shown in Table S1.

Sodium-ion half cells performance

Fig. 4a displays the first three CV curves of NTHC-1150 half-cell, which was tested between 0 and 2 V at a scanning rate of 0.1 mV s^{-1}. Three small reduction peaks at 1.3, 0.9 and 0.5 V (*vs.* Na/Na^+) appear only in the first

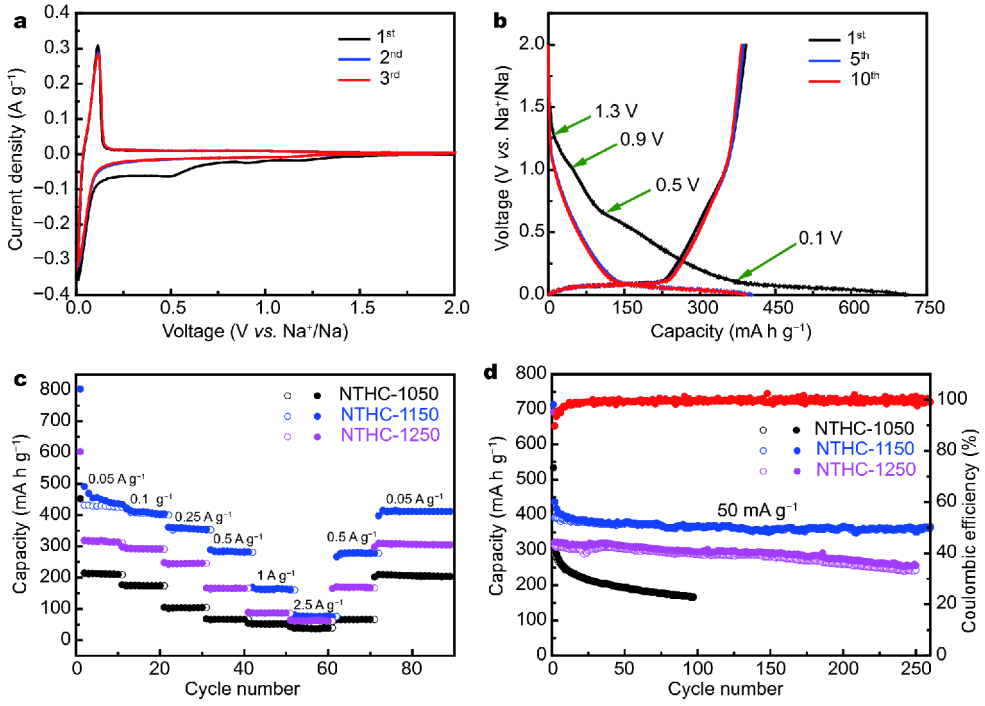

Figure 4 (a) The first three CV curves of NTHC-1150 in 0–2 V at a sweep speed of 0.1 mV^{-1}; (b) GCD curves of NTHC-1150 at the 1, 5, 10 cycles between 0 and 2 V at a current density of 50 mA g^{-1}; (c) rate capability of NTHCs at different current densities; (d) cycle performance of NTHCs at 50 mA g^{-1}.

cathodic scan, suggesting that irreversible reactions occur with the formation of SEI film, associated with decomposition of electrolyte on the electrode surface [49]. Moreover, a pair of typical redox peaks about 0.114/0.01 V in the low potential region is related to the reversible insertion/extraction of Na^+ ions between quasi-graphite layers. Fig. 4b shows the GCD curves of NTHC-1150 at a current density of 50 mA g^{-1} for 1st, 5th and 10th cycle. The first GCD curve has four distinct discharge platforms, and the longest discharge platform was at the 0.1 V, which is consistent with the CV result. Fig. 4c shows the rate capability of NTHCs. It is worth noting that NTHC-1150 shows the better rate performance than that of NTHC-1050 and NTHC-1250. Specifically speaking, NTHC-1150 delivers reversible capacities of 419.5, 361.1, 288.8, 168.3, 80.2 and 74.6 mA h g^{-1} at current densities of 50, 100, 250, 500, 1000 and 2500 mA g^{-1}, respectively. When the current density is reset to 500 and 50 mA g^{-1}, the electrode capacity recovers to 277.9 and 411.5 mA h g^{-1}, which indicates the NTHC-1150 has a good rate capability as well as excellent tolerance to rapid Na^+ insertion and extraction.

Fig. 4d shows the cycling performance of the NTHCs electrodes at a constant current density of 50 mA g^{-1}. Compared with NTHC-1050, -1250, NTHC-1150 has the best cycle performance and reversible capacity, the NTHC-1150 electrode still maintains a high reversible capacity of 366.6 mA h g^{-1} after 260 cycles, corresponding to the second cycle discharge capacity retention rate of 83.9%. Coulombic efficiencies of the NTHC-1050, -1150 and -1250 are 53.7%, 54.9%, 45%, respectively. The comparison of half-cell performance is also shown in Table S2. The main reason of NTHC-1150 with the best performance may be the larger interlayer spacing and the N heteroatoms, in which big interlayer spacing reduces the ion diffusion rate, and N heteroatoms can increase the conductivity.

SIHCs performance

Before each NTHC-1150//APDC SIHC device was assembled and tested, NTHC-1150 electrode was pre-processed in half-cell (i.e. *vs.* Na/Na^+). The NTHC-1150 anode was firstly galvanostatically tested ten cycles at 50 mA g^{-1} between 0–2 V *vs.* Na/Na^+, and then discharged to a cut-off voltage of 0.01 V *vs.* Na/Na^+. Then a SIHC was assembled with APDC (the electrochemical properties are shown in Fig. S4) as the cathode and the NTHC-1150 as the anode. According to the capacity

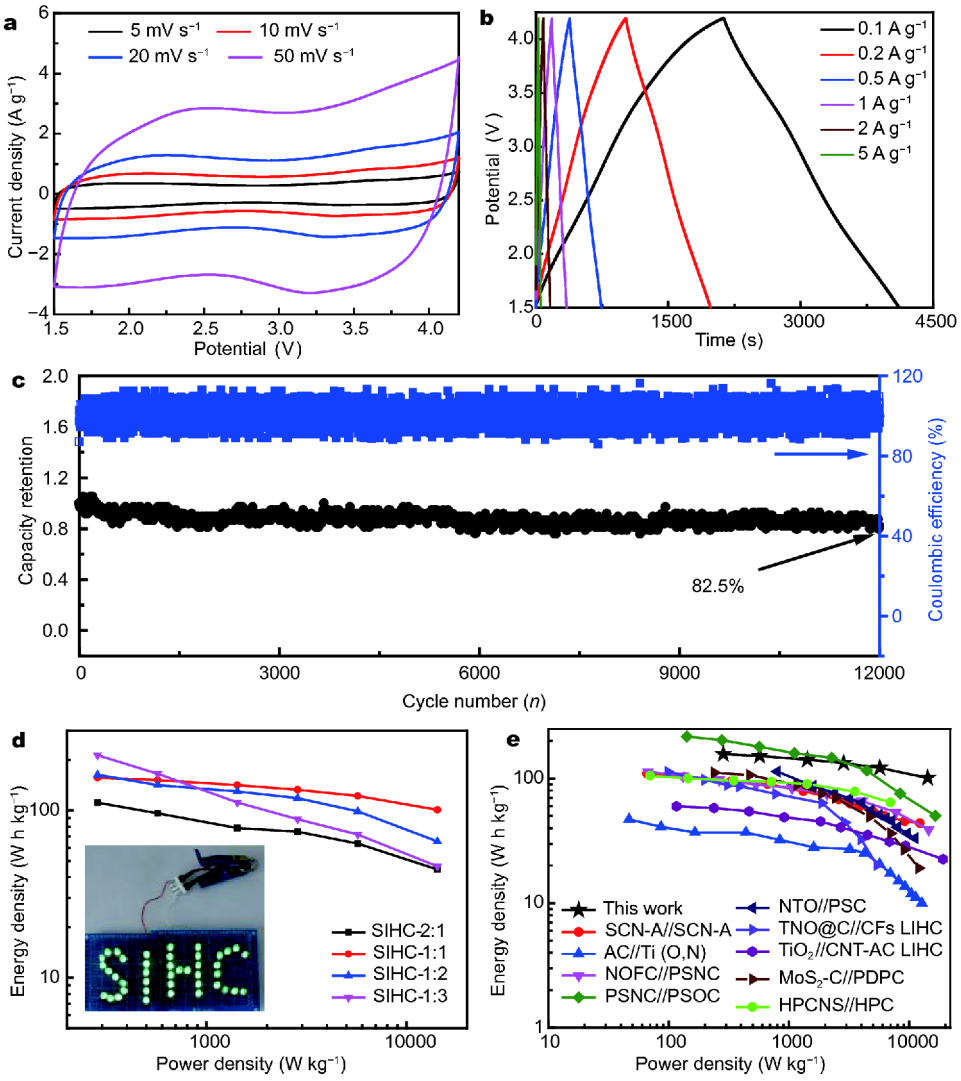

Figure 5 (a) CV of NTHC-1150//APDC SIHC at a different sweep speeds; (b) GCD curves of NTHC-1150//APDC SIHC; (c) rate performance of NTHC-1150//APDC SIHC; (d) ragone plots of NTHC-1150//APDC SIHCs with the different mass ratios; (e) ragone plots of various hybrid capacitors [50–54].

balance between the NTHC-1150 anode and the APDC cathode, their mass ratio varies from 2:1 to 1:3 (the detailed electrochemical properties are shown in Figs. S5 and S6). With increasing mass ratio of NTHC-1150 and APDC, the energy density initially increases and then decreases to 1:1. The optimal performance of the SIHC device is shown in Fig. 5. Fig. 5a shows the CV curves with different scan rates in the voltage window of 1.5–4.2 V. The device shows a rectangular shape, which indicates the capacity is ascribed to capacitive behavior. Fig. 5b is the GCD curves at different current densities in the voltage window of 1.5–4.2 V, which exhibits quasi-symmetric triangular-shape (Fig. S7), further indicating the good combination between the insertion/extraction of sodium ions in NTHC-1150 anode and APDC cathode.

The cycling stability of the NTHC-1150//APDC dual-carbon SIHC was firstly investigated at a current density of 2 A g^{-1}. First of all, using a maximum voltage window of 1.5–4.2 V, compared with the initial capacity, the device showed the capacity retention rate of 58.5% after 10,000 cycles. When we employed a smaller voltage window of 1.5–3.5 V, the capacity retention rate increased to 74% after 10,000 cycles (Fig. S8). When the device was firstly activated for 200 cycles at 200 mA g^{-1} in voltage window of 1.5–3.5 V (Fig. S9), and then the cycling performance was tested at 2 A g^{-1} in voltage window of

1.5–3.5 V, the capacity retention rate further increased to 84% after 10,000 cycles and 82.5% after 12,000 cycles, as shown in Fig. 5c. Fig. S10 shows the EIS plots of NTHC-1150//APDC SIHC at different cycles (initial state and after 10,000 cycles). The high frequency region has the charge transfer resistance controlled by kinetic, while the low frequency region is determined by the diffusion of sodium ions in the carbon material. It is shown that the resistance of NTHC-1150//APDC SIHC after 10,000 cycles was still lower than that of the initial state, which indicates NTHC-1150//APDC SIHC has a good charge transfer performance. Ragone plots of NTHC-1150//APDC SIHC with different mass ratios are shown in Fig. 5d, where the power densities and specific energy were calculated based on the total mass of anode and cathode active materials. The optimal device with the mass ratio of 1:1 is able to achieve a maximum energy density of 100.9 W h kg^{-1} as well as a maximum power density of 14,250 W kg^{-1}. This SIHC can be assembled to drive a 3 V light-emitting diode (LED) with a "SIHC" pattern (Fig. S11), which implies the potential for the application of the SIHC. In comparison, the energy and power densities of reported SCN-A//SCN-A, AC//Ti (O, N)-MP-NWs, NIC-NOFC//PSNC [50], PSNC//PSOC, NTO//PSC [51], TNO@C//CFs [52], TiO_2/CNT-AC, MoS_2-C//PDPC [53], HPCNS//HPC [54] as well as our optimized SIHC device are plotted together in Fig. 5e. The ragone plot makes NTHC-1150//APDC SIHC (marked as black star) very competitive in practical application. As shown in Fig. 5e, although the maximal energy density of our device is not the highest value compared with the previous reported SIHCs [27], the decrease slope of energy density with the increase of power density is the best. The outstanding electrochemical performance of NTHC-1150//APDC SIHC can be ascribed to the following three reasons: (i) The NTHC-1150 anode possesses a suitable interlayer spacing with Na^+ ions insertion/extraction. (ii) The nanostructure of the electrode materials contributes to the transfer of ions and the contact of the electrolyte. (iii) The dual-carbon electrodes from the same raw material may be more conducive for dynamic and structural stability matching, resulting in the enhancement of the overall performance of the hybrid device.

CONCLUSIONS

In conclusion, we have prepared NTHC-1150 anode and APDC cathode with similar one-dimensional structure from low cost PANI. In the 0–2 V voltage window, the assembled sodium ion half-cell with NTHC-1150 as anode can exhibit a high reversible capacity of 419.5 mA h g^{-1} at 0.05 A g^{-1} and an excellent rate performance of 74.6 mA h g^{-1} at 2.5 A g^{-1}, and shows a good cycle performance. On this basic, the as-fabricated SIHC with the optimal mass matching can exhibit a maximum energy density of 133.0 W h kg^{-1} at 2850 W kg^{-1} and still can remain 100.9 W h kg^{-1} at 14250 W kg^{-1}. At testing voltage window of 1.5–3.5 V, the hybrid capacitor achieves outstanding cycling stability even after 12000 cycles. Therefore, it is believable that dual-carbon SIHC will cause widespread concern for further commercial application due to abundant raw materials, environmental friendliness and simple manufacturing.

Received 1 September 2017; accepted 14 October 2017; published online 27 November 2017

1 An C, Liu X, Gao Z, *et al.* Filling and unfilling carbon capsules with transition metal oxide nanoparticles for Li-ion hybrid supercapacitors: towards hundred grade energy density. Sci China Mater, 2017, 60: 217–227
2 Hou H, Xu Q, Pang Y, *et al.* Efficient storing energy harvested by triboelectric nanogenerators using a safe and durable all-solid-state sodium-ion battery. Adv Sci, 2017, 4: 1700072
3 Chen F, Gong AS, Zhu M, *et al.* Mesoporous, three-dimensional wood membrane decorated with nanoparticles for highly efficient water treatment. ACS Nano, 2017, 11: 4275–4282
4 Hwang JY, Myung ST, Sun YK. Sodium-ion batteries: present and future. Chem Soc Rev, 2017, 46: 3529–3614
5 Liu L, Shen B, Jiang D, *et al.* Watchband-like supercapacitors with body temperature inducible shape memory ability. Adv Energy Mater, 2016, 6: 1600763
6 Sevilla M, Mokaya R. Energy storage applications of activated carbons: supercapacitors and hydrogen storage. Energy Environ Sci, 2014, 7: 1250–1280
7 Wang Y, Song Y, Xia Y. Electrochemical capacitors: mechanism, materials, systems, characterization and applications. Chem Soc Rev, 2016, 45: 5925–5950
8 Lukatskaya MR, Dunn B, Gogotsi Y. Multidimensional materials and device architectures for future hybrid energy storage. Nat Commun, 2016, 7: 12647
9 Sun Y, Hu X, Yu JC, *et al.* Morphosynthesis of a hierarchical MoO_2 nanoarchitecture as a binder-free anode for lithium-ion batteries. Energ Environ Sci, 2011, 4: 2870
10 Li W, Siqin GW, Zhu Z, *et al.* Electrochemical properties of niobium and phosphate doped spherical Li-rich spinel $LiMn_2O_4$ synthesized by ion implantation method. Chin Chem Lett, 2017, 28: 1438–1446
11 Yang XY, Xu JJ, Bao D, *et al.* High-performance integrated self-package flexible Li-O_2 battery based on stable composite anode and flexible gas diffusion layer. Adv Mater, 2017, 29: 1700378
12 Zhang P, He M, Xu S, *et al.* The controlled growth of porous δ-MnO_2 nanosheets on carbon fibers as a bi-functional catalyst for rechargeable lithium-oxygen batteries. J Mater Chem A, 2015, 3: 10811–10818
13 Yao Y, Zeng L, Hu S, *et al.* Binding $S_{0.6}Se_{0.4}$ in 1D carbon nanofiber with CS bonding for high-performance flexible Li-S batteries and Na-S batteries. Small, 2017, 13: 1603513
14 Yu J, Hu YS, Pan F, *et al.* A class of liquid anode for rechargeable

batteries with ultralong cycle life. Nat Commun, 2017, 8: 14629
15 Sottmann J, Di Michiel M, Fjellvåg H, *et al.* Chemical structures of specific sodium ion battery components determined by operando pair distribution function and X-ray diffraction computed tomography. Angew Chem Int Ed, 2017, 56: 11385–11389
16 Ji BF, Zhang F, Wu NZ, *et al.* A dual-carbon battery based on potassium-ion electrolyte. Adv Energy Mater, 2017
17 Zhang SQ, Wang M, Zhou ZM, *et al.* Multifunctional electrode design consisting of 3D porous separator modulated with patterned anode for high-performance dual-ion batteries. Adv Funct Mater, 2017
18 Wang R, Jin D, Zhang Y, *et al.* Engineering metal organic framework derived 3D nanostructures for high performance hybrid supercapacitors. J Mater Chem A, 2017, 5: 292–302
19 Xia Q, Yang H, Wang M, *et al.* High energy and high power lithium-ion capacitors based on boron and nitrogen dual-doped 3D carbon nanofibers as both cathode and anode. Adv Energ Mater, 2017, 451: 1701336
20 Zhang S, Li C, Zhang X, *et al.* High performance lithium-ion hybrid capacitors employing Fe_3O_4-graphene composite anode and activated carbon cathode. ACS Appl Mater Interfaces, 2017, 9: 17136–17144
21 Sun X, Zhang X, Liu W, *et al.* Electrochemical performances and capacity fading behaviors of activated carbon/hard carbon lithium ion capacitor. Electrochim Acta, 2017, 235: 158–166
22 Xu N, Sun X, Zhao F, *et al.* The role of pre-lithiation in activated carbon/$Li_4Ti_5O_{12}$ asymmetric capacitors. Electrochim Acta, 2017, 236: 443–450
23 Chen Z, Yuan Y, Zhou H, *et al.* 3D nanocomposite architectures from carbon-nanotube-threaded nanocrystals for high-performance electrochemical energy storage. Adv Mater, 2014, 26: 339–345
24 Thangavel R, Moorthy B, Kim DK, *et al.* Pushing the energy output and cyclability of sodium hybrid capacitors at high power to new limits. Adv Energy Mater, 2017, 7: 1602654
25 Dong J, Jiang Y, Li Q, *et al.* Pseudocapacitive titanium oxynitride mesoporous nanowires with iso-oriented nanocrystals for ultrahigh-rate sodium ion hybrid capacitors. J Mater Chem A, 2017, 5: 10827–10835
26 Lim E, Jo C, Kim MS, *et al.* Hybrid supercapacitors: high-performance sodium-ion hybrid supercapacitor based on Nb_2O_5@carbon core-shell nanoparticles and reduced graphene oxide nanocomposites. Adv Funct Mater, 2016, 26: 3553–3553
27 Ding J, Wang H, Li Z, *et al.* Peanut shell hybrid sodium ion capacitor with extreme energy-power rivals lithium ion capacitors. Energy Environ Sci, 2015, 8: 941–955
28 Chen Z, Augustyn V, Jia X, *et al.* High-performance sodium-ion pseudocapacitors based on hierarchically porous nanowire composites. ACS Nano, 2012, 6: 4319–4327
29 Jian Z, Raju V, Li Z, *et al.* A high-power symmetric Na-ion pseudocapacitor. Adv Funct Mater, 2015, 25: 5778–5785
30 Liu S, Cai Z, Zhou J, *et al.* Nitrogen-doped TiO_2 nanospheres for advanced sodium-ion battery and sodium-ion capacitor applications. J Mater Chem A, 2016, 4: 18278–18283
31 Xu D, Chen C, Xie J, *et al.* A hierarchical N/S-codoped carbon anode fabricated facilely from cellulose/polyaniline microspheres for high-performance sodium-ion batteries. Adv Energ Mater, 2016, 6: 1501929
32 Cao Y, Xiao L, Sushko ML, *et al.* Sodium ion insertion in hollow carbon nanowires for battery applications. Nano Lett, 2012, 12: 3783–3787
33 Xiao L, Cao Y, Henderson WA, *et al.* Hard carbon nanoparticles as high-capacity, high-stability anodic materials for Na-ion batteries. Nano Energy, 2016, 19: 279–288
34 Wang RT, Lang JW, Yan XB. Effect of surface area and heteroatom of porous carbon materials on electrochemical capacitance in aqueous and organic electrolytes. Sci China Chem, 2014, 57: 1570–1578
35 Yin J, Xia X, Xiang L, *et al.* Conductivity and polarization of carbonaceous nanotubes derived from polyaniline nanotubes and their electrorheology when dispersed in silicone oil. Carbon, 2010, 48: 2958–2967
36 Yin J, Xia X, Xiang L, *et al.* The electrorheological effect of polyaniline nanofiber, nanoparticle and microparticle suspensions. Smart Mater Struct, 2009, 18: 095007
37 Wang F, Wang X, Chang Z, *et al.* A quasi-solid-state sodium-ion capacitor with high energy density. Adv Mater, 2015, 27: 6962–6968
38 Stejskal J, Sapurina I, Trchová M, *et al.* Oxidation of aniline: polyaniline granules, nanotubes, and oligoaniline microspheres. Macromolecules, 2008, 41: 3530–3536
39 He D, Wu Y, Xu BQ. Formation of 2,3-diaminophenazines and their self-assembly into nanobelts in aqueous medium. Eur Polymer J, 2007, 43: 3703–3709
40 Xiao L, Cao Y, Xiao J, *et al.* A soft approach to encapsulate sulfur: polyaniline nanotubes for lithium-sulfur batteries with long cycle life. Adv Mater, 2012, 24: 1176–1181
41 Yan D, Yu C, Zhang X, *et al.* Nitrogen-doped carbon microspheres derived from oatmeal as high capacity and superior long life anode material for sodium ion battery. Electrochim Acta, 2016, 191: 385–391
42 Trchová M, Matějka P, Brodinová J, *et al.* Structural and conductivity changes during the pyrolysis of polyaniline base. Polym Degrad Stab, 2006, 91: 114–121
43 Li S, Cheng C, Liang HW, *et al.* 2D porous carbons prepared from layered organic-inorganic hybrids and their use as oxygen-reduction electrocatalysts. Adv Mater, 2017, 29: 1700707
44 Li Z, Bommier C, Chong ZS, *et al.* Mechanism of Na-ion storage in hard carbon anodes revealed by heteroatom doping. Adv Energy Mater, 2017, 7: 1602894
45 Yan D, Xu X, Lu T, *et al.* Reduced graphene oxide/carbon nanotubes sponge: a new high capacity and long life anode material for sodium-ion batteries. J Power Sources, 2016, 316: 132–138
46 Jiang C, Wang J, Chen Z, *et al.* Nitrogen-doped hierarchical carbon spheres derived from MnO_2-templated spherical polypyrrole as excellent high rate anode of Li-ion batteries. Electrochim Acta, 2017, 245: 279–286
47 Yue J, Epstein AJ. XPS study of self-doped conducting polyaniline and parent systems. Macromolecules, 1991, 24: 4441–4445
48 Yang M, Zhou Z. Recent breakthroughs in supercapacitors boosted by nitrogen-rich porous carbon materials. Adv Sci, 2017, 4: 1600408
49 Zhang B, Ghimbeu CM, Laberty C, *et al.* Correlation between microstructure and Na storage behavior in hard carbon. Adv Energ Mater, 2016, 6: 1501588
50 Ding J, Li Z, Cui K, *et al.* Heteroatom enhanced sodium ion capacity and rate capability in a hydrogel derived carbon give record performance in a hybrid ion capacitor. Nano Energ, 2016, 23: 129–137
51 Li H, Peng L, Zhu Y, *et al.* Achieving high-energy-high-power

density in a flexible quasi-solid-state sodium ion capacitor. Nano Lett, 2016, 16: 5938–5943
52 Wang X, Shen G. Intercalation pseudo-capacitive $TiNb_2O_7$@carbon electrode for high-performance lithium ion hybrid electrochemical supercapacitors with ultrahigh energy density. Nano Energy, 2015, 15: 104–115
53 Wang R, Wang S, Peng X, *et al.* Elucidating the intercalation pseudocapacitance mechanism of MoS_2-carbon monolayer interoverlapped superstructure: toward high-performance sodium-ion-based hybrid supercapacitor. ACS Appl Mater Interfaces, 2017, 9: 32745–32755
54 Niu J, Liang J, Shao R, *et al.* Tremella-like N,O-codoped hierarchically porous carbon nanosheets as high-performance anode materials for high energy and ultrafast Na-ion capacitors. Nano Energy, 2017, 41: 285–292

Acknowledgements This work was supported by the National Natural Science Foundation of China (21573265, 21673263 and 51501208), and the 13th Five-Year Strategic Planning of Chinese Academy of Sciences.

Author contributions Ding Y and Yan X conceived and designed the experiments; Ding Y and Yang B synthesized and characterized the materials; Ding Y, Chen J and Zhang L performed the data analysis; Ding Y wrote the manuscript; Li J participated in the manuscript editing; Li Y analyzed the results and revised the manuscript. All authors contributed to the general discussion.

Conflict of interest The authors declare that they have no conflict of interest.

Supplementary information Supporting data are available in the online version of the paper.

Yongqiang Ding is currently studying in the School of Physics and Technology of Lanzhou University. His research is focused on the use of carbon-based materials in sodium ion hybrid capacitors.

Yali Li received her Bachelor and Master Degrees of Science both from Lanzhou University, China and Doctoral Degree of Engineering from Saitama University, Japan. From 2009.01 to 2012.03, she worked at the Nanyang Technological University, Singapore as a Research Fellow. She currently is an associate professor at School of Physical Science & Technology, Lanzhou University. Now, her main research interest is focused on renewable energy devices, including Si nanostructure-based solar cells and energy storage devices.

Xingbin Yan received his PhD degree in physical chemistry from Lanzhou Institute of Chemical Physics (LICP) in 2005. Afterwards he worked at the Nanyang Technological University as a Research Fellow and University of Lyon as a Postdoctoral Researcher. Professor Yan is now the director of Laboratory of Clean Energy Chemistry and Materials, LICP, Chinese Academy of Sciences. His research group works on energy storage devices including supercapacitors and rechargeable batteries. For details, please see the lab website: www.licp.cas.cn/yxbz.

纳米管状硬碳作为负极材料构建高性能钠离子混合电容器

丁永强[1,2], 杨兵军[1], 陈江涛[1], 张莉[3], 栗军帅[2], 李亚丽[2*], 阎兴斌[1*]

摘要 由于具有良好的能量和功率特性, 以及钠资源丰富和成本低, 钠离子混合电容器(SIHCs)在大规模储能应用中受到了广泛的关注. 然而, 负极材料缓慢的动力学严重限制了SIHC器件的整体电化学性能. 本文报道了一种纳米管状硬碳(NTHC)负极材料用于制作高性能SIHC, 这种材料是通过高温碳化(1150°C)聚苯胺(PANI)得到的. 结果显示, NTHC作为钠离子半电池负极, 在0.05 A g^{-1}下具有高的可逆容量(419.5 mA h g^{-1})和优异的倍率性能. 利用HCNT作为负极和高容量活性炭(APDC)作为正极组装的SIHC器件在2850 W kg^{-1}的功率密度下表现出的能量密度高达133.0 W h kg^{-1}, 当功率密度高达14250 W kg^{-1}条件下器件能量密度仍然保持100.9 W h kg^{-1}; 在1.5–3.5 V的电位范围内, 器件展现出良好的循环稳定性, 在2 A g^{-1}条件下循环12000次后其容量保持率高达82.5%.

